

UCLA

UCLA Previously Published Works

Title

Micro-zircon inclusions in accessory minerals reveal more complete magma compositional evolution records

Permalink

<https://escholarship.org/uc/item/9gk5c9h0>

Journal

Contributions to Mineralogy and Petrology, 177(12)

ISSN

0010-7999 1432-0967

Authors

Bell, Elizabeth A

Kirkpatrick, Heather M

Publication Date

2022-11-28

DOI

10.1007/s00410-022-01979-6

Supplemental Material

<https://escholarship.org/uc/item/9gk5c9h0#supplemental>

Data Availability

The data associated with this publication are in the supplemental files.

Peer reviewed

Word count: 6500

1
2 **Micro-zircon inclusions in accessory minerals reveal more complete magma compositional evolution**
3 **records**

4 Elizabeth A. Bell^{*,1}, Heather M. Kirkpatrick^{1,2}

5 ¹Dept. of Earth, Planetary, & Space Sciences, UCLA, Los Angeles, CA 90095, USA

6 ²now at Dept. of Earth and Planetary Sciences, Harvard University, Cambridge, MA 02138, USA

7 *Corresponding author: ebell21@ucla.edu

8 **Abstract**

9 Trace elements in magmatic zircon exhibit characteristic trends during magma compositional evolution.
10 Zircon geochemistry presents the advantage over whole rock geochemistry of showing progressive
11 'snapshots' of accompanying melt chemistry during magma crystallization, and in situ methods such as
12 LA-ICPMS and SIMS can provide multiple analyses in zoned zircons for higher resolution of magmatic
13 processes. However, one limitation is that zircon is typically a late-crystallizing phase, leaving much of the
14 magmatic history unrecorded. Using the CAMECA *ims1290* ion microprobe with Hyperion-II ion source,
15 we explore whether micro-zircon (ca. 5-40 μm) captured by relatively early-crystallizing magmatic
16 accessory minerals can meaningfully enhance the interpretations of zircon trace element records of
17 magmatic evolution in two granites from Southern California: the La Posta 2-mica granite and the granite
18 of Butler Peak (Big Bear Lake Intrusive Suite). We find that contamination of the inclusion measurement
19 by major structural constituents of the host phase is a problem for most measurements, but that species
20 which are not structural components of the host phases follow typical magmatic zircon trace element
21 evolution trends. Compared to free grains from a mineral separate, zircon inclusions in ilmenite and
22 apatite from the La Posta 2-mica granite are on average lower in Hf, recording plausible extensions of

23 these magmatic evolution trends to earlier periods in magma evolution. Free zircons from the granite of
24 Butler Peak's mineral separate form a more complex story, recording both mixing between Cretaceous
25 magmas derived from different depths (based on their U/Yb and Eu/Eu* behavior) and inheritance of
26 older Mesozoic to Proterozoic zircon. Most zircon inclusions in Butler Peak magnetite and ilmenite are
27 chemically like the apparently shallow magma-derived Cretaceous zircons in the free matrix, while a small
28 proportion of the included zircon resemble more closely the apparently deeper magma or the inherited
29 grains.

30 **Introduction**

31 Magmatic zircon displays characteristic trace element relationships related to magma evolution
32 by crystallization and fractionation (e.g., Claiborne et al., 2010). For example, these typically identified
33 crystallization patterns include a negative relationship between Ti and Hf which – since Ti concentration
34 relates directly to crystallization temperature (Watson and Harrison, 2005; Ferry and Watson, 2007)–
35 demonstrates an increase in Hf with progressive zircon crystallization from a melt (Claiborne et al., 2010).
36 Because zircon tends to saturate relatively late in the crystallization history of most magmas (e.g.,
37 Boehnke et al., 2013), zircon trace element patterns can typically only provide information about the later
38 stages of magma compositional evolution. Other methods, or trace element evaluation of other accessory
39 phases, may be necessary for probing earlier melt history. At the same time, the lower-Hf, less evolved
40 portions of the zircon population may display substantially different trace element behavior than the
41 more evolved populations (e.g., Th/U versus Hf slopes). Further exploring the early history of the zircon
42 suite is limited by the number of zircons with unaltered magmatic chemistry (judged by, e.g., Sm/La or
43 the light rare earth index, LREE-I; Hoskin, 2005 and Bell et al., 2016, respectively) which fall at relatively
44 high Ti and low Hf. Given that LREE-I tends to increase (i.e. appear more magmatic) during magma
45 evolution the conservative use of this filter will also limit the number of analyses available at the less-
46 evolved end of the zircon distribution.

47

48 Other trace element ratios that typically vary with increasing Hf in shallow to mid crustal magmas
49 include decreasing Th/U, decreasing Eu/Eu*, increasing U/Yb, and increasing Yb/Gd with increasing Hf.
50 Although decreasing Eu/Eu* can be tied to plagioclase fractionation, the other ratios are probably affected
51 by a variety of other co-crystallizing minerals. Zircon Th/U also differs by magma composition, with mafic-
52 intermediate high-temperature melts yielding zircon with higher average Th/U than more felsic melts
53 (Kirkland et al., 2015). Whether the high Th/U displayed in the less-evolved, low-Hf portions of granite
54 zircon suites is related to the more universally high Th/U in mafic zircon suites is unclear. In granite zircon
55 suites with a large range in Hf contents, the slope of the Th/U vs Hf relationship may differ significantly
56 with Hf, often forming a concave-up relationship (e.g., Claiborne et al., 2010; Bell and Kirkpatrick, 2021)
57 with the less evolved (low-Hf) zircons showing near-vertical slope vs Hf. In some cases, deviation from
58 these expected patterns for many of these trace element ratios may suggest significant crustal
59 assimilation or magma mixing (e.g., Langenheim et al., 2021; Bell and Kirkpatrick, 2021).

60 Instead of searching for the relatively rare, less evolved, low-Hf zircon among the typically sized
61 grains picked from mineral separates (usually >50-100 μm), one alternative for probing the earlier magma
62 evolution history may be to search for zircon inclusions that were trapped in other minerals shortly after
63 zircon formation, and before they could be mantled by relatively larger volumes of later zircon grown
64 from more evolved melt. Relatively early-forming minerals, such as many ferromagnesian phases or Fe-
65 Ti oxides, may be able to capture and armor zircon early in its growth history, providing an additional
66 archive that should in theory be more biased towards the early magmatic history. Zircon trapped by later
67 accessory phases may show less bias and might help identify the latest parts of the magmatic history as
68 recorded in zircon. In order to investigate this possibility, we have undertaken analyses of Ti, REE, Hf, Th,
69 and U on a suite of 5-40 μm zircon hosted as either inclusions or embaying phases by magnetite, ilmenite,
70 sphene, apatite, and monazite in two silicic granites from southern California.

71 **Samples & Methods**

72 Granite samples were crushed to <425 μm and panned in water. The heavy mineral separate was
73 then further sorted using a hand magnet followed by a Franz isodynamic magnetic separator. Free grains
74 of magnetite, ilmenite, zircon, monazite, and apatite were picked from the various magnetic separates,
75 mounted in epoxy, and polished with silicon carbide grinding paper and diamond paste to expose an
76 interior surface. Electron imaging using a Vega 3 XMU scanning electron microscope (SEM) fitted with an
77 energy dispersive x-ray detector (EDS) was used to find and identify inclusions within the accessory
78 mineral grains. We focused on the granite of Butler Peak (San Bernardino Mountains) and La Posta
79 muscovite-biotite granite (see Fig. 1) here due to the ubiquity of zircon inclusions in oxide and phosphate
80 accessory minerals. All analyzed zircon inclusions are tabulated in Table 1.

81 *La Posta muscovite-biotite granite:* The La Posta muscovite-biotite unit is the innermost, evolved
82 unit at the core of the Cretaceous La Posta pluton in the Peninsular Ranges Batholith, southern California
83 (e.g., Clinkenbeard and Walawender, 1989). It is a fine-grained 2-mica, ilmenite series granite with
84 isotopic evidence for some assimilation of metasediment (Walawender et al., 1990). Ilmenite, apatite,
85 and monazite picked from the mineral separate contain abundant 5-20 μm zircon inclusions (Bell et al.,
86 2022) either fully enclosed or embaying the grain edge(see Fig. S1). Bell et al. (2022) concluded, based on
87 comparing mutual fully-enclosed inclusion proportions (see Table S2), that zircon likely began to crystallize
88 before ilmenite and apatite in this magma and monazite began crystallizing after ilmenite, leading to
89 potential sampling of different stages of magmatic history with inclusions in ilmenite potentially sampling
90 earlier stages of melt history. U-Pb dating suggests no pervasive inheritance of older zircon (Kirkpatrick
91 et al., 2020).

92 *Granite of Butler Peak:* The granite of Butler Peak is the innermost, evolved, peraluminous unit at
93 the core of the Cretaceous Big Bear Lake Intrusive Suite in the San Bernardino Mountains, southern

94 California (Barth et al, 2016). It is a fine-grained 2-mica magnetite-series granite also containing ilmenite
95 and monazite. Zircon U-Pb dating of the unit by previous studies reveals some inheritance of Proterozoic
96 country rock zircon as well as scattered >100 Ma zircon potentially related to earlier Phanerozoic magmas
97 (Barth et al., 2016; Bell et al., 2022). A survey of mineral inclusions (by Bell et al., 2022) in various accessory
98 minerals of the Butler Peak unit reveal abundant 5-20 μm and occasionally larger crystals of zircon either
99 fully included in or embaying magnetite, ilmenite, and monazite. Bell et al. (2022) concluded on the basis
100 of comparing mutual fully-enclosed inclusion proportions that zircon likely began to crystallize before the
101 Fe-Ti oxides in the magma and monazite began crystallizing after the Fe-Ti oxides (see Table S2). This
102 suggests that small zircon inclusions trapped within monazite will preferentially sample the later stages
103 of magma history, while small zircon inclusions trapped within the oxides may preferentially sample
104 earlier stages. In addition to textural observations of inclusion phases, Bell et al. (2022) also undertook ion
105 microprobe U-Pb dating for the free zircons in the granite of Butler Peak, and we refer to their results to
106 distinguish inherited from neo-grown free zircon.

107 *Ion microprobe trace element measurements*

108 Trace element measurements were undertaken using the CAMECA *ims1290* ion microprobe at
109 UCLA with the Hyperion-II ion source (Liu et al., 2018). Following the analytical procedures of Schmitt and
110 Vazquez (2006), a suite of trace elements including P, Ti, Y, the REE, Hf, Th, and U were collected using ^{30}Si
111 for normalization. Mg, Mn, and $^{57}\text{Fe}/^{30}\text{Si}$ were also collected to check for contamination by surrounding
112 host phases, as typical for zircon trace element measurements (e.g., Schmitt and Vazquez, 2006). As an
113 additional check, we also use $^{96}\text{Zr}/^{30}\text{Si}$ and $^{44}\text{Ca}/^{30}\text{Si}$ as guides for placement on zircon vs surrounding
114 phases.

115 Analyses were run at low mass-resolving power (<1600) for maximum signal throughput. To suppress
116 molecular interferences, a -100V offset was applied to the sample stage and additional peak stripping for

117 REE oxide interferences was carried out offline. The NIST-610 standard glass was used to calculate relative
118 sensitivity factors for all elements, and accuracy was checked against the 91500 zircon compositional
119 standard (Wiedenbeck et al., 2004). While zircon trace element measurements are typically run with
120 primary beam intensities sufficient to yield >100,000 counts per second (cps) secondary signal on ^{30}Si
121 (typically 3-5 nA O_3^- on the *ims1290*), we used O_3^- primary beams between 750 pA and 1.4 nA, with
122 resulting ^{30}Si signals ranging from the high 1000s to 10,000s cps. The field aperture was kept relatively
123 open at a width of 5000 μm for all standard analyses and analyses on larger free-mounted zircons in the
124 grain mounts. For zircon inclusions in other phases, the field aperture was narrowed on a case-by-case
125 basis to values between 3000 and 650 μm to limit contamination by surrounding materials. We undertook
126 measurements of many zircon inclusions in Butler Peak magnetite with a static beam, while for most other
127 inclusions we used a 2 μm raster with a corresponding raster added in the secondary beam to compensate
128 (i.e., DTOS).

129 **Results**

130 For inclusions with a small dimension of 10 μm or larger, it was generally possible to place the
131 analysis spot on the included zircon with minimal or no overlap with the host phase (see Figs. 2, S1). For
132 inclusions with small dimensions under 10 μm , this was less consistently achieved. The incident angle of
133 the primary beam imparts some horizontal movement during digging of the crater, leading to the partial
134 host overlap in some cases (see Figs. 2, S1).

135 Regardless of crater overlap, analyses were consistently contaminated with major constituents of
136 the host phase – virtually all analyses on magnetite contained unusually high $^{57}\text{Fe}/^{30}\text{Si}$ compared to the
137 larger zircon picked freely from the mineral separate. All analyses in ilmenite hosts and most in magnetite
138 hosts show Ti contents much higher than inclusions in other phases or free zircon within the same unit.
139 Likewise, P and LREE contents are much higher for zircon included in apatite and monazite hosts compared

140 to free zircon or oxide-hosted zircon. For micro-zircon inclusions in oxide and sphene, LREE-I values
141 typically fall above 30, suggesting unaltered and uncontaminated magmatic REE chemistry (Bell et al.,
142 2016). Most free zircon have similarly high LREE-I values. Zircons in monazite and apatite mostly though
143 not all have LREE-I<30.

144 **Discussion**

145 Micro-zircon inclusions from their respective rocks fit well into the magmatic evolution histories
146 defined by free zircons in the same rocks after filtering for alteration and contamination. Contamination
147 by structural constituents of the host phase is widespread, and is assessed in Figure 3 for the La Posta
148 micro-zircon. Figure 4 defines groups of neo-grown magmatic zircon vs inherited zircon from the granite
149 of Butler Peak, and these groups are used in Figure 5 which shows host phase contamination in the micro-
150 zircon vs free zircon from the granite of Butler Peak. Inclusions in ilmenite contain Ti concentrations that
151 lead to geologically unrealistic calculated Ti-in-zircon temperatures, and most inclusions in magnetite also
152 have Ti contamination from the host grain. Oxide-hosted micro-zircon show high LREE-I mostly falling into
153 the primary magmatic composition range (Bell et al., 2016), and the inclusions in La Posta ilmenite fit well
154 into the relatively simple shallow fractionation trends shown by free zircons picked from the heavy
155 mineral separate for that magma (Bell and Kirkpatrick, 2021). They fall preferentially toward the low-Hf,
156 less-evolved portion of the zircon melt history. Free zircons in the granite of Butler Peak record a more
157 complex evolution, with U-Pb results from Bell et al. (2022) defining inherited vs neo-grown magmatic
158 zircons among the sampled free zircons. Neo-grown magmatic zircons are classified into three groups
159 (see Figure 4): we define two lower-Hf groups by contrasting P contents (high-P >200ppm and low-P
160 <200ppm) and note that their very different U/Yb and Eu/Eu* may suggest origins in separate melts (e.g.,
161 Bell and Kirkpatrick, 2021; discussed further below). A high-Hf group consistent with more evolved melt
162 may be linked to the high-Hf neo-grown zircons identified previously in highly evolved granites from the
163 Big Bear Lake Intrusive Suite by Barth et al. (2016). These high-Hf zircons are also more isotopically

164 homogeneous than zircon derived from a number of less-evolved magmas (i.e., low-Hf, higher-T zircon),
165 suggesting the mixing of several less evolved magmas to form the more highly evolved melts in the suite
166 (Barth et al., 2016). As a caveat to the discussion of micro-zircon inclusions versus “free” zircons, our
167 sample processing procedures do not allow us to constrain whether the larger zircons were included in
168 larger, brittle host grains (e.g., biotite) before sample crushing.

169 *Micro-zircon inclusions vs free zircon*

170 We plot the light rare earth element index (LREE-I; Bell et al., 2016, 2019), a measure of REE
171 contamination in zircon, against common contaminants in the included and free zircon in Figures 3 and 5.
172 On Figure 3 and 5 we include low cutoff values for altered REE chemistries suggested by several studies.
173 LREE-I < 30 is based on the strong increase in light element, P, and U-Th contaminants below LREE-I = 30
174 in the Archean-Hadean Jack Hills zircons, which have undergone metamorphism in a quartzite host rock,
175 with contamination of cracks and void space by secondary Fe-Ti oxides and phosphates (e.g., Bell et al.,
176 2015; Rasmussen et al., 2011). We also include on these figures the more conservative LREE-I < 60 cutoff
177 suggested by Bell et al. (2019) for out-of-context zircon based on several modern granitoids with varying
178 degrees of alteration. We define LREE-I < 30 as the cutoff for alteration for the purposes of this manuscript
179 given the specifically oxide and phosphate contaminants similar to the Jack Hills case. Most free zircon
180 appear unaltered and uncontaminated based on LREE-I and low quantities of Ti, Mn, Fe, Mg, and P.
181 $^{96}\text{Zr}/^{30}\text{Si}$ of ~ 2-2.5 appears typical for free zircon as well as most included zircon. This quantity was not
182 measured for several of the free zircon in La Posta (Bell and Kirkpatrick, 2021). Inclusions in ilmenite show
183 the clearest contamination trends for La Posta with increasing Ti, Fe, Mn, and Mg with decreasing LREE-I,
184 although inclusions in apatite also show increasing P contamination with lower LREE-I (Figure 3).
185 Alteration or contamination trends with LREE-I are unclear in the granite of Butler Peak (Figure 5).

186 For analyses that may retain some aspects of uncontaminated primary REE chemistry based on
187 the LREE-I, we plot both free zircons and zircon inclusions for the same magmatic unit in trace element
188 quantities that show characteristic trends during magma evolution (Figures 6, 7). We plot for comparison
189 the inclusions with low LREE-I which appear to reflect alteration or contamination with other REE-rich
190 phases. We note differing behaviors for the La Posta inclusions vs the Butler Peak inclusions. Compared
191 to free zircons in La Posta, the La Posta inclusions tend to cluster toward lower Hf contents. Although
192 their relationship to free zircons is somewhat obscured by the higher error bars – particularly for Eu/Eu*
193 – the inclusions tend to fit in to the relatively simple trends displayed by free zircons (Figure 6). These
194 include decreasing Th/U and Eu/Eu* with increasing Hf, along with increasing U/Yb vs Hf. We also observe
195 anti-correlated Yb/Gd vs Th/U and U/Yb vs Eu/Eu*. Butler Peak free zircons display more complicated
196 Eu/Eu* and U/Yb behavior (Figure 4). Low-P free zircons are more likely to display high U/Yb and typically
197 have higher Eu/Eu* than the high-P and high-Hf free zircon. While many zircon inclusions in oxides show
198 high Eu/Eu*, they mostly have low U/Yb more similar to most high-P free zircons. The inclusions also
199 mostly appear to contain >200 ppm P. This may suggest their derivation from higher-Eu/Eu* (i.e., less
200 evolved) melts in the high-P group. Some of the high-U/Yb, high-Eu/Eu* inclusions may be consistent with
201 either the low-P free zircon or with inherited zircon, although the latter show less systematic chemistry.
202 We must also evaluate the role of host phase contamination and the feasibility of eliminating it while
203 retaining useful signals for the other geologically interesting trace elements.

204 *Challenges and trade-offs in eliminating host phase contamination*

205 Even in cases where later SEM imaging shows no visible overlap of the analysis pit with the host,
206 we consistently observe significant contamination by host phase major element constituents (see Figs. 3,
207 5) even with the field aperture narrowed to the point of significant signal reduction in many cases. The
208 secondary ion signals from our zircon inclusions are much weaker than those for typical zircon trace
209 element measurements using this method (for ^{30}Si typically several 100,000 counts per second; e.g.,

210 Schmitt and Vazquez, 2006), owing to the lower primary beam intensity and narrow field aperture (2000-
211 650 μm). For many of our inclusions, we observe signals of $\leq 10,000$ cps for ^{30}Si . Consequently, low-
212 abundance trace elements like the LREE have notably higher error bars in our inclusions compared to
213 higher-signal measurements on larger zircons. For example, Nd in our La Posta inclusion zircons shows
214 average external 1 s.d. error bars of 31% (see Table S1), as opposed to 16% in larger La Posta zircons
215 measured by Bell and Kirkpatrick (2021). For many inclusions these limitations begin to stretch the limits
216 of data usability, especially for calculating the LREE-I and Eu/Eu* (see Figs. 3, 5). Because of the signal
217 limitations that will be necessary for cutting out all host phase contamination in zircons of this size, usable
218 REE pattern measurements may need to be made separately from usable measurements of Ti in, for
219 instance, ilmenite- or rutile-hosted inclusions – should usable measurements of Ti be possible in such
220 samples. A more systematic study to determine inclusion size, optimal primary beam current, and optimal
221 field aperture width is beyond the scope of this study but will likely be necessary in order to determine
222 the feasibility of Ti measurements in ilmenite-hosted zircon. For measuring trace elements that are not
223 structural constituents of the surrounding phases, this method seems to suffice in measuring, for example,
224 magmatic REE patterns (based on LREE-I) for zircon inclusions in oxide minerals and even, in rare cases,
225 phosphate minerals that fit into the granitoid's free-grown zircon trace element trends.

226 Our primary beam tuning for these analyses (critical/Gaussian beam) has proven suitable for
227 other micro-grain applications, such as U-Pb dating (e.g., Liu et al., 2011 for a duoplasmatron ion source
228 on a similar instrument; Marquardt et al., 2022 with UCLA *ims1290* with Hyperion-II as used in this study),
229 where contaminating common Pb from surrounding phases may adversely affect the U-Pb isotopic date.
230 However, Pb is a structural component of relatively few minerals, so this may not be a good analogy for,
231 e.g., measuring trace Ti in a zircon embedded in ilmenite. Further refinement of this technique may allow
232 more probing of elements that are minor to major constituents of the host phases. There is some reason
233 for optimism: for example, several zircon inclusions hosted in Butler Peak magnetite contain <10 ppm Ti

234 and only mildly elevated $^{57}\text{Fe}/^{30}\text{Si}$ relative to free zircon from the mineral separate. One each of the
235 monazite- and apatite-hosted zircons in the granite of Butler Peak also show LREE-I > 30. Out of context,
236 this LREE-I is suggestive of primary magmatic chemistry (Bell et al., 2016), although LREE-I > 60 and
237 $(\text{La}/\text{Sm})_N > 10$ presents a clearer case for primary magmatic chemistry (Bell et al., 2019 and Hoskin, 2005
238 respectively) and are not displayed by any phosphate-hosted zircons in this study. We also note that the
239 spurious Ti concentrations in ilmenite-hosted zircon measured by ion probe in this study are likely less
240 than that which would be imparted by secondary fluorescence on an electron microprobe (Wark and
241 Watson, 2006).

242 An alternative source of contamination – as opposed to the liberation of material directly from
243 the host by the margins of the primary beam – is surface contamination of the inclusion by surrounding
244 host material during polishing. Longer pre-sputter intervals during which the ion beam rasters the surface
245 of the inclusion and cleans off potential host-derived surface contamination may be helpful in future
246 studies, but imposes the additional danger of sputtering away the actual zircon inclusion before analysis
247 can take place, especially since the depth of the zircon beneath the mount surface is unclear. For the
248 smaller zircon inclusions <5 μm , these long pre-sputter times may sputter a significant amount of the
249 analyzable volume of the sample itself, and further testing for feasibility will be needed.

250 For completeness, we evaluate the alternative hypothesis that the high abundance of host phase
251 major constituents in our measurements reflect not analytical contamination but rather diffusion into the
252 micro-zircon inclusions in amounts that would be geologically unreasonable in other settings. Because
253 diffusivities of Ti and several REE in zircon are known, we can calculate characteristic diffusion length
254 scales for these species in zircon. For the sake of argument, we consider a case where the magmas were
255 held until geologically recently at the lowest magmatic temperature recorded by a grain with “clean”
256 LREE-I and magmatic Th/U (assuming $\alpha_{\text{TiO}_2}=0.7$: 621°C in LP6, 631°C in BB14) and the approximate age of
257 these granitoids (La Posta: ca. 100 Ma, Kirkpatrick et al., 2020; Butler Peak: ca. 80 Ma, Barth et al., 2016;

258 Bell et al., 2022). For zircon held at 650°C for 100 Ma, using the diffusivity of Ti in zircon from Cherniak
259 and Watson (2007) and the diffusivities of Yb, Dy, and Sm in zircon from Cherniak et al. (1997), we
260 calculate characteristic diffusion lengths of 1×10^{-6} μm for Ti and 1×10^{-4} , 9×10^{-5} , and 3×10^{-6} μm for Yb, Dy,
261 and Sm respectively. These chemical species would in summary be essentially immobile in neo-grown
262 magmatic zircons from these granites, even if they were held at only slightly subsolidus temperatures
263 since their crystallization. Recent re-evaluation of Ti diffusivity has suggested significant anisotropy in
264 zircon, with much faster diffusion parallel to the c-axis (Bloch et al., 2022). Redoing this calculation using
265 these revised diffusivity estimates however suggest a characteristic diffusion length of only 0.1 μm parallel
266 to the c-axis – a potential volumetrically significant concern for the smallest of the inclusions documented
267 here (e.g., <2 μm). Analyzing inclusions this small is currently beyond the capabilities of this method, but
268 may become possible with further development.

269 A related scenario involving inheritance of older zircon which had been held at higher
270 metamorphic temperatures may also be useful to consider. Approximately 15% of zircons dated from the
271 granite of Butler Peak by Barth et al. (2016) were ca. 1.0-1.2 Ga grains inherited from Precambrian country
272 rock, and a further 20% were inherited Mesozoic grains. The presence of a significant minority of inherited
273 zircons in the granite of Butler Peak is also corroborated by Bell et al. (2022). By contrast, inherited zircon
274 is rarer in the La Posta unit (Kirkpatrick et al., 2020). If inherited zircons were mantled by other accessory
275 phases as inclusions, we could envision a scenario where they were held at higher temperatures for longer
276 periods of time. For residence in the lower crust at high geothermal gradient (following Shankland and
277 Ander, 1983), we redo the calculations for residence at 900°C for 1 Ga. In this case, we calculate
278 characteristic diffusion lengths of ca. 14, 8, and 1 μm for Yb, Dy, and Sm respectively. While earlier results
279 for c-perpendicular diffusion (Cherniak and Watson, 2007) would suggest a characteristic length of 0.1 μm
280 for Ti, the characteristic distance for c-parallel diffusion (Bloch et al., 2022) would be hundreds of μm . For
281 5-40 μm zircon grains like these inclusions, 1 Ga residence at high-temperature metamorphic conditions

282 might indeed impart significant diffusion of the REE and Ti. This is probably unrealistic in most continental
283 settings, especially in the depressed geothermal gradients typically associated with arcs (e.g., Shankland
284 and Ander, 1983). More specific predictions would require modeling for specific zircon geometries,
285 timescales, and thermal conditions (e.g., Bloch et al., 2022). Based on these considerations, we assume
286 that the high Ti, Fe, P, and LREE in most of our inclusions are indeed due to analytical contamination rather
287 than diffusion, particularly for those which appear to fit into the magmatic evolution trends of their
288 respective neo-grown free zircon populations. There is however some possibility for REE and Ti mobility
289 of inherited Precambrian micro-zircon in the granite of Butler Peak.

290 *Supplementing the magma compositional evolution record*

291 5-40 μm zircon included in magnetite and ilmenite which display apparently primary LREE-I tend
292 to show multiple markers of deriving from the less evolved portion of the zircon crystallization history
293 displayed by the larger, freely picked zircon in the same rocks (see Figs. 6, 7). On average they are lower
294 in Hf and Yb/Gd and higher in Th/U than their larger counterparts, which are typical of zircon crystallized
295 earlier in less evolved melt (e.g., Claiborne et al., 2010). They plausibly fit into the evolution histories
296 outlined by larger free zircon in their host rocks, although the simpler evolution suggested by La Posta
297 zircons provides easier interpretations than the more complex patterns of Butler Peak zircons.

298 *La Posta:*

299 Micro-zircon inclusions in oxide and phosphate hosts of the La Posta muscovite-biotite granite
300 range in their LREE-I, but those with apparently primary magmatic chemistry are very similar in trace
301 element trend behavior to the larger, non-included zircon picked from mineral separates by Bell and
302 Kirkpatrick (2021). They display the expected (e.g. Claiborne et al., 2010) decreases in Th/U and Eu/Eu*
303 and increase in U/Yb with Hf. The inclusions showing LREE-I > 30 fit well into the distribution defined by

304 the larger, free zircons. They are slightly higher in U/Yb compared to the free zircon, but this effect is not
305 significant considering error.

306 The clustering of ilmenite-hosted zircon toward the low-Hf end of the range for larger zircons is
307 mirrored by the ilmenite-hosted zircons' lower Yb/Gd and higher Th/U and appears to suggest their
308 crystallization on average in the less evolved melt than reflected by the majority of zircon crystallization
309 in this granite. Only one zircon each that is hosted in apatite and monazite appears to have magmatic
310 chemistry based on LREE-I, but these also fall toward the lower-Hf end of the free zircon distribution.
311 Their slope in Eu/Eu* and Th/U vs Hf may be helpful for better understanding the trace element behavior
312 of zircon in less evolved melts or the early histories of zircon crystallization in granite. For example, the
313 characteristic decrease in zircon Th/U with increasing Hf is absent in some mafic-intermediate units from
314 the Western Zone of the Peninsular Ranges Batholith (Bell and Kirkpatrick, 2021), which the authors
315 speculate may be due to either particular minerals which fractionate Th from U not coexisting with zircon
316 in these melts or saturating too late to affect the earlier portion of zircon crystallization histories.
317 Alternatively, since fluid saturation level or fluid loss during crystallization can also affect Th/U
318 fractionation (e.g., Keppler and Wyllie, 1991), these different Th/U behaviors during melt evolution might
319 relate to fluid saturation levels in the host magma. By contrast to the zircons with >10,000ppm Hf, which
320 show a shallow negative trend between Th/U and Hf, below 10,000ppm Hf the zircon Th/U value increase
321 precipitously with decreasing Hf. In the context of the higher-Hf zircon they appear to form a concave-up
322 curve, but if only the lowest-Hf zircon were available to measure the trend may not be clear, much like
323 that for the intermediate Western Zone magmas (Bell and Kirkpatrick, 2021). This may suggest that a
324 muddled relationship between Th/U and Hf may indeed be characteristic of early stages of melt evolution
325 – even in more evolved granitoids like this relatively silicic peraluminous granite. In these more evolved
326 silicic melts, the earliest stages of melt evolution will likely be most accessible with micro-zircon inclusions
327 captured by other phases early in the melt history, while other small growing zircon crystals are

328 subsequently armored by more zircon, often disguising or hiding the signature of the earlier-formed core
329 material. The latter is especially true when there is no clear cathodoluminescence evidence for earlier
330 cores mantled by later comagmatic zircon.

331 *Butler Peak:*

332 Free zircons in the granite of Butler Peak display a more complex evolution potentially involving
333 magma mixing, along with a significant population of inherited zircons, as outlined above. Two lower-Hf
334 groups derived from less evolved melts yield contrasting high-P and low-P zircon (with a cutoff defined
335 ~ 200 ppm). A smaller high-Hf group of zircon probably represents more evolved melt, and these grains
336 also show higher P > 200 ppm. P content in zircon is partially a function of melt ASI (Burnham and Berry,
337 2017), given the higher P contents in peraluminous melts (ASI > 1) due to the suppression of apatite
338 saturation (Pichavant et al., 1992). While zircon P contents > 750 ppm are nearly always a marker for
339 origins in an S-type granite (Zhu et al., 2020), many peraluminous granites do yield zircon with lower P
340 contents (Burnham and Berry, 2017). The significance of < 200 ppm vs 200-500 ppm P in the two Butler
341 Peak zircon groups is not entirely clear from a melt ASI perspective. The granite of Butler Peak is
342 peraluminous enough to have crystallized primary muscovite (e.g., Barth et al., 2016), and one primary
343 muscovite inclusion is identified in both zircon and ilmenite hosts in the rock (Bell et al., 2022; see also
344 Table S2), but given the rarity of muscovite inclusions in zircon the melt ASI throughout the window of
345 zircon crystallization is not entirely clear. The combination of higher Eu/Eu* and higher U/Yb in the low-
346 P group (Fig. 4d) suggests that the high- and low-P zircon groups do not fall on the same shallow magmatic
347 fractionation trend (Bell and Kirkpatrick, 2021). Following the discussion of Bell and Kirkpatrick (2021),
348 magmatic fractionation at a relatively shallow level (i.e., garnet absent) should produce a negative
349 relationship between U/Yb and Eu/Eu* as observed in the La Posta zircons studied here (e.g., Fig. 6f) and
350 as suggested by most high-P zircon in the granite of Butler Peak (e.g., Fig. 7f). Assimilation of sediments
351 or similarly low-U/Yb materials will also tend to yield magmatic evolution similar to shallow fractionation

352 in U/Yb vs Eu/Eu* (Bell and Kirkpatrick, 2021). Sediment assimilation would also lead to higher ASI, which
353 might be consistent with the higher zircon P (although both metaluminous and peraluminous melts can
354 lead to zircons with this range of P contents; Zhu et al., 2020). This would suggest that the high-P and
355 high-Hf zircons are more consistent with growth in a magma like the present Butler Peak unit. Sediment
356 assimilation would however in most cases be at odds with the higher redox displayed by the high-P group
357 compared to the other free zircons (Fig. 4b), given the ubiquity of organic carbon in many sediments which
358 typically leads to lower oxygen fugacity. The high-P group may then be more likely to simply represent
359 shallow peraluminous magma, with either little sediment assimilation or only assimilation of carbon-poor
360 sediments. The low-P zircons mostly falling at both higher U/Yb and Eu/Eu* may suggest their derivation
361 from either deeper or more water-rich sources (through the suppression of plagioclase crystallization).
362 Because Th/Yb responds similarly to U/Yb for depth but lacks the response to magmatic water (which
363 owes to U's redox behavior; Langmuir, 1978; Sverjensky and Lee, 2010), the similar behavior of Th/Yb vs
364 Eu/Eu* (see Fig. S4) suggests that this effect is related to depth. We focused on U/Yb for the main text
365 given the co-crystallization of monazite with zircon in both studied granites, which can complicate the
366 Th/Yb vs Eu/Eu* relationship (Bell and Kirkpatrick, 2021). Finally, the high-Hf zircon group is intermediate
367 between the low-P and high-P groups in U/Yb and Th/Yb (Figs. 7, S4) and appears consistent with mixing
368 between the two less-evolved magmas represented by the high- and low-P groups. This interpretation is
369 also consistent with Barth et al. (2016)'s model for the mixed, more isotopically homogeneous melts
370 represented by the higher-Hf zircons in units at the core of the Big Bear Lake Intrusive Suite.

371 Many micro-zircon inclusions in magnetite and ilmenite fall at lower U/Yb and higher P and are
372 largely consistent with the high-P group of free zircons. However, they fall on average at higher Eu/Eu*,
373 which may suggest they do preferentially draw from the earlier history of the high-P melt. Several
374 inclusions in magnetite (and one hosted in ilmenite) fall at higher Eu/Eu* and U/Yb and would be
375 consistent on this basis with either the low-P neo-grown zircons or many of the inherited zircons which

376 share this chemistry. Most of the inclusions have >200ppm P, unlike the low-P group, and so may be more
377 likely to be inherited. However, they have lower Yb/Gd than the majority of the inherited free zircon.
378 Given that the inclusions tend to fall toward both lower Yb/Gd and higher Th/U than free zircon, this could
379 reflect growth in less evolved melts than the other inherited grains. If these inclusions are inherited zircon,
380 whether their host magnetite and ilmenite are also inherited presents an interesting question: peritectic
381 phase entrainment may be an important magmatic evolution process and may involve ilmenite in
382 particular (e.g., Villaros et al., 2009; Stevens et al., 2007). It is possible that studies of micro-zircon
383 inclusions in oxides could help to elucidate this process on a grain-by-grain basis.

384 *Further implications for magmatic zircon studies*

385 In Bell et al.'s (2019) survey of alteration chemistry in zircon from Neoproterozoic to Cenozoic
386 granitoids that have undergone varying degrees of hydrothermal circulation or metamorphism following
387 emplacement, they compared the REE pattern in zircon as quantified by the LREE-I to common
388 contaminant species (Mg, Mn, Fe, Ti, P) in an effort to recommend "cutoff" values for altered (low LREE-
389 I) vs unaltered, primary chemistry (high LREE-I). While zircon from some highly altered granites (Bell et
390 al., 2019) and the Jack Hills metasediments (Bell et al., 2016) show strong relationships between LREE-I
391 and species related to contamination by secondary phosphates and Fe-Ti oxides, many granitoid zircons
392 show no clear relationship between LREE-I and light element contaminants or P. A handful of zircons
393 within each of the studied rocks, for instance, displayed outlier high Ti contents but otherwise
394 unproblematic LREE-I. The authors speculated that this was due to contamination by consumption of
395 micro-oxide inclusions during ion probe analysis. This idea is borne out by data from our magnetite- and
396 ilmenite-hosted zircon, which may display high LREE-I and REE-Hf-Th-U chemistry very similar to trends in
397 the larger free zircon picked from the mineral separate but nearly always display geologically
398 unreasonable Fe, Mn, and Ti contents. It may be feasible in future studies to use the REE-Hf-Th-U data
399 for such analyses – where they appear reasonably similar to non-contaminated analyses – and forego

400 using only the contaminated Ti for geological interpretations. Similarly, for apatite- and monazite-hosted
401 zircon with accompanying low LREE-I, it may be feasible to provisionally interpret Ti temperatures if the
402 Ti and Fe contents of the analyses appear reasonable compared to other zircons in the population at hand.
403 In this way some additional data can be extracted from zircon trace element datasets, even if interpreted
404 only provisionally.

405 Another interesting question that remains outstanding is how common micro-zircon inclusions
406 are in magmatic minerals. Apatite inclusions, for instance, will consistently occur in the margins of major
407 and accessory mineral phases likely due to the 'pileup' of slow-diffusing phosphate complexes against
408 growing mineral surfaces in silicate melts (e.g. Green and Watson, 1982; Harrison and Watson, 1984). The
409 higher diffusivity of Zr compared to P_2O_5 in hydrous magmas (Zhang et al., 2010) probably inhibits the
410 pileup effect for zircon in most silicate magmas. Relatively low Ti-in-zircon crystallization temperatures
411 for free zircon and high-LREE-I monazite- and apatite-hosted zircon in these two units suggest high melt
412 water contents, further suggesting that Zr 'pileup' is less likely to be the cause of the widespread zircon
413 inclusions. The zircon inclusions in the La Posta and Butler Peak granites also tend to lack the regular host
414 face-parallel orientations of apatite inclusions inferred to form by pileup (e.g., Green and Watson, 1982;
415 Harrison and Watson, 1984).

416 In contrast to the origins of zircon inclusions in these two granites, it might be possible to create
417 widespread micro-zircon inclusions in drier melts that do incur a 'pileup effect' for Zr against growing
418 mineral faces. In addition to lower Zr diffusivity due to lower melt water contents, Zr pileup and zircon
419 capture could also be promoted by much faster phenocryst growth rates relative to Zr diffusion. It may
420 be that zircon is a more common inclusion phase in other accessory (or major) minerals in, for instance,
421 volcanic rocks due to lower water contents or fast growth of phenocrysts. If so, then investigations of
422 micro-zircon inclusions by ion microprobe may form an important part of lava chemical evolution studies
423 in the future.

424 Conclusions

425 Analysis of micro-zircon inclusions can supplement the record of magmatic evolution available in
426 larger zircon picked from mineral separates. We document two case studies of zircon-rich Fe-Ti oxides
427 and phosphate minerals in highly silicic granites and show that apart from structural constituents of host
428 phases, trace element measurements on $\geq 5 \mu\text{m}$ zircon hosted by oxide and phosphate minerals can yield
429 interpretable chemical evolution patterns when analyzed using the Hyperion-II ion source. More stringent
430 filtering of host material necessary for measuring host structural constituents at trace level in the zircon
431 inclusions may yet be possible, but may not be compatible with simultaneous measurement of lower-
432 abundance trace elements such as LREE and Eu.

433 In one case (La Posta), the relatively simple chemical evolution suggested by larger free zircon from the
434 mineral separate is enhanced by the majority early-forming zircon inclusions, fleshing out the less evolved
435 portion of magmatic compositional evolution. In a second case (Butler Peak), the free zircon represent a
436 more complex history with a) magma mixing between a shallowly fractionating higher-P melt and a deeper
437 (based on U/Yb) low-P melt, and b) inheritance of zircon which appears to be mainly high-U/Yb and high-
438 Eu/Eu*. The zircon inclusions fall mainly in the apparently shallow high-P zircon group, at higher average
439 Eu/Eu* consistent with deriving from less-evolved melts. Some oxide-hosted grains fall into the higher-
440 U/Yb chemistry, and their trace element patterns are overall more consistent with inheritance. Further
441 refinement of the technique may allow more probing of elements at trace level in zircon but more
442 abundant in the host – as shown by several magnetite-hosted zircons with <10 ppm Ti and only mildly
443 elevated Fe along with monazite- and apatite-hosted zircons displaying LREE-I values suggestive of
444 primary magmatic chemistry.

445 Acknowledgments

446 We thank Ming-Chang Liu for assistance with ion probe measurements. Discussions with Melanie Barboni
447 and Mark Harrison were very helpful in developing the study. We thank Josh Rosera and an anonymous
448 reviewer for comments which helped improve the manuscript, and Othmar Muntener for his editorial
449 handling. The ion microprobe laboratory at UCLA is partially supported by a grant from NSF-EAR's
450 Instrumentation and Facilities Program (1734856).

451

452 **References**

453 Barth, A. P., Wooden, J. L., Mueller, P. A., & Economos, R. C. (2016). Granite provenance and intrusion in
454 arcs: Evidence from diverse zircon types in Big Bear Lake Intrusive Suite, USA. *Lithos*, 246, 261-278.

455 Bell, E. A., Boehnke, P., Barboni, M., & Harrison, T. M. (2019). Tracking chemical alteration in magmatic
456 zircon using rare earth element abundances. *Chemical Geology*, 510, 56-71.

457 Bell, E. A., Boehnke, P., & Harrison, T. M. (2016). Recovering the primary geochemistry of Jack Hills zircons
458 through quantitative estimates of chemical alteration. *Geochimica et Cosmochimica Acta*, 191, 187-202.

459 Bell, E. A., Boehnke, P., Harrison, T. M., & Wielicki, M. M. (2018). Mineral inclusion assemblage and detrital
460 zircon provenance. *Chemical Geology*, 477, 151-160.

461 Bell, E. A., Boehnke, P., Hopkins-Wielicki, M. D., & Harrison, T. M. (2015). Distinguishing primary and
462 secondary inclusion assemblages in Jack Hills zircons. *Lithos*, 234, 15-26.

463 Bell, E. A., & Kirkpatrick, H. M. (2021). Effects of crustal assimilation and magma mixing on zircon trace
464 element relationships across the Peninsular Ranges Batholith. *Chemical Geology*, 586, 120616.

465 Boehnke, P., Watson, E. B., Trail, D., Harrison, T. M., & Schmitt, A. K. (2013). Zircon saturation re-revisited.
466 *Chemical Geology*, 351, 324-334.

- 467 Burnham, A. D., & Berry, A. J. (2017). Formation of Hadean granites by melting of igneous crust. *Nature*
468 *Geoscience*, 10(6), 457-461.
- 469 Cherniak, D. J., Hanchar, J. M., & Watson, E. B. (1997). Rare-earth diffusion in zircon. *Chemical Geology*,
470 134(4), 289-301.
- 471 Cherniak, D. J., & Watson, E. B. (2007). Ti diffusion in zircon. *Chemical Geology*, 242, 470-483.
- 472 Claiborne, L. L., Miller, C. F., Wooden, J. L., & Mazdab, F. K. (2010). Trace element composition of igneous
473 zircon: temporal, thermal, and compositional record of magmatic processes in the Spirit Mountain
474 Batholith, Nevada. *Contrib Mineral Petr*, 60, 511-531.
- 475 Clinkenbeard, J. P., & Walawender, M. J. (1989). Mineralogy of the La Posta pluton: Implications for the
476 origin of zoned plutons in the eastern Peninsular Ranges batholith, southern and Baja California. *American*
477 *Mineralogist*, 74(11-12), 1258-1269.
- 478 Ferry, J. M., & Watson, E. B. (2007). New thermodynamic models and revised calibrations for the Ti-in-
479 zircon and Zr-in-rutile thermometers. *Contributions to Mineralogy and Petrology*, 154(4), 429-437.
- 480 Green, T. H., & Watson, E. B. (1982). Crystallization of apatite in natural magmas under high pressure,
481 hydrous conditions, with particular reference to 'orogenic' rock series. *Contributions to Mineralogy and*
482 *Petrology*, 79(1), 96-105.
- 483 Harrison, T. M., & Watson, E. B. (1984). The behavior of apatite during crustal anatexis: equilibrium and
484 kinetic considerations. *Geochimica et Cosmochimica Acta*, 48(7), 1467-1477.
- 485 Hoskin, P. W. (2005). Trace-element composition of hydrothermal zircon and the alteration of Hadean
486 zircon from the Jack Hills, Australia. *Geochimica et cosmochimica acta*, 69(3), 637-648.
- 487 Jennings, C.W.; Gutierrez, C.I. (2010). Geologic Map of California. California Department of Conservation,

- 488 California Geological Survey: Sacramento, CA, USA, 2010.
- 489 Keppler, H., & Wyllie, P. J. (1991). Partitioning of Cu, Sn, Mo, W, U, and Th between melt and aqueous
490 fluid in the systems haplogranite-H₂O-HCl and haplogranite-H₂O-HF. *Contributions to Mineralogy and*
491 *Petrology*, 109(2), 139-150. <https://doi.org/10.1007/BF00306474>
- 492 Kirkland, C. L., Smithies, R. H., Taylor, R. J. M., Evans, N., & McDonald, B. (2015). Zircon Th/U ratios in
493 magmatic environs. *Lithos*, 212, 397-414.
- 494 Kirkpatrick, H., T.M. Harrison, E.A. Bell, M.-C.- Liu, F. Tissot, S.A. MacLennan, and M. Ibanez-Mejia (2020),
495 Are Zr stable isotopes tracking magmatic differentiation in the zoned La Posta pluton?, Abstract V032-
496 0004 presented at 2020 Fall Meeting, AGU, San Francisco, CA.
- 497 Langenheim, V. E., Vazquez, J. A., Schmidt, K. M., Guglielmo, G., & Sweetkind, D. S. (2021). Influence of
498 pre-existing structure on pluton emplacement and geomorphology: The Merrimac plutons, northern
499 Sierra Nevada, California, USA. *Geosphere*, 17(2), 455-478.
- 500 Langmuir, D. (1978). Uranium solution-mineral equilibria at low temperatures with applications to
501 sedimentary ore deposits. *Geochimica et Cosmochimica Acta*, 42(6), 547-569.
- 502 Liu, M. C., McKeegan, K. D., Harrison, T. M., Jarzebinski, G., & Vltava, L. (2018). The Hyperion-II radio-
503 frequency oxygen ion source on the UCLA ims1290 ion microprobe: Beam characterization and
504 applications in geochemistry and cosmochemistry. *International Journal of Mass Spectrometry*, 424, 1-9.
- 505 Liu, Y., Li, X. H., Li, Q. L., Tang, G. Q., & Yin, Q. Z. (2011). Precise U-Pb zircon dating at a scale of < 5 micron
506 by the CAMECA 1280 SIMS using a Gaussian illumination probe. *Journal of Analytical Atomic*
507 *Spectrometry*, 26(4), 845-851.
- 508 Marquardt, M., Barboni, M., & Bell, E. A. (2022). Exploring the Geochemical, Geochronologic, and Thermal
509 History of HED Meteorites Using Zircon. *LPI Contributions*, 2678, 2420.

- 510 Rasmussen, B., Fletcher, I. R., Muhling, J. R., Gregory, C. J., & Wilde, S. A. (2011). Metamorphic
511 replacement of mineral inclusions in detrital zircon from Jack Hills, Australia: Implications for the Hadean
512 Earth. *Geology*, 39(12), 1143-1146.
- 513 Schmitt, A. K., & Vazquez, J. A. (2006). Alteration and remelting of nascent oceanic crust during continental
514 rapture: Evidence from zircon geochemistry of rhyolites and xenoliths from the Salton Trough, California.
515 *Earth and Planetary Science Letters*, 252(3-4), 260-274.
- 516 Shankland, T. J., & Ander, M. E. (1983). Electrical conductivity, temperatures, and fluids in the lower crust.
517 *Journal of Geophysical Research: Solid Earth*, 88(B11), 9475-9484.
- 518 Stevens, G., Villaros, A., & Moyen, J.-F. (2007). Selective peritectic garnet entrainment as the origin of
519 geochemical diversity in S-type granites. *Geology*, 35(1), 9-12. <https://doi.org/10.1130/G22959A.1>
- 520 Sverjensky, D. A., & Lee, N. (2010). The great oxidation event and mineral diversification. *Elements*, 6(1),
521 31-36.
- 522 Villaros, A., Stevens, G., Moyen, J.-F., & Buick, I. S. (2009). The trace element compositions of S-type
523 granites: evidence for disequilibrium melting and accessory phase entrainment in the source.
524 *Contributions to Mineralogy and Petrology*, 158(4), 543-561. [https://doi.org/10.1007/s00410-009-0396-](https://doi.org/10.1007/s00410-009-0396-3)
525 3
- 526 Walawender, M. J., Gastil, R. G., Clinkenbeard, J. P., McCormick, W. V., Eastman, B. G., Wemicke, R. S., ...
527 & Smith, B. M. (1990). Origin and evolution of the zoned La Posta-type plutons, eastern Peninsular. The
528 nature and origin of Cordilleran magmatism, 174, 1.
- 529 Wark, D.A., and Watson, E.B., 2006, TitaniQ: A titanium-in-quartz geothermometer: *Contributions to*
530 *Mineralogy and Petrology*, v. 152, p. 743–754, doi:10.1007/s00410-006-0132-1.

531 Watson, E. B., & Harrison, T. M. (2005). Zircon thermometer reveals minimum melting conditions on
 532 earliest Earth. *Science*, 308(5723), 841-844.

533 Wiedenbeck, M., Hanchar, J. M., Peck, W. H., Sylvester, P., Valley, J., Whitehouse, M., ... & Zheng, Y. F.
 534 (2004). Further characterisation of the 91500 zircon crystal. *Geostandards and Geoanalytical Research*,
 535 28(1), 9-39.

536 Zhang, Y., Ni, H., & Chen, Y. (2010). Diffusion data in silicate melts. *Reviews in Mineralogy and*
 537 *Geochemistry*, 72(1), 311-408.

538 Zhu, Z., Campbell, I. H., Allen, C. M., & Burnham, A. D. (2020). S-type granites: Their origin and distribution
 539 through time as determined from detrital zircons. *Earth and Planetary Science Letters*, 536, 116140.

540

541

542 **Table Captions:**

Sample	Host	Length (µm)	Width (µm)	Host Overlap?	Field aperture width (µm)	Other Notes
<i>La Posta Muscovite-Biotite Granite</i>						
Lp6ilm-1.1z1	Sphene (mantling ilmenite)	10	20	No	3000	High Ti-Fe, altered LREE-I
Lp6ilm-1.1z2@1	Sphene (mantles ilmenite)	15	20	No	2000	High Ti-Fe, good LREE-I
Lp6ilm-1.1z2@2	Sphene (mantles ilmenite)	15	20	Completely off	1000	High Ti-Fe, altered LREE-I
Lp6ilm-1.1z2@3	Sphene (mantles ilmenite)	15	20	No	1000	High Ti-Fe, good LREE-I
Lp6ilm-1.19z1@1	Ilmenite	10	20	Slight	1000	High Ti-Fe, good LREE-I
Lp6ilm-1.19z1@2	Ilmenite	10	20	No	1000	High Ti-Fe, good LREE-I

Lp6ilm-1.19z1@3	Ilmenite	10	20	Slight	1000	Hi Ti, lo Fe, good LREE-I
Lp6ilm-1.31z1@1	Ilmenite	10	25	No	1000	High Ti-Fe, altered LREE-I
Lp6ilm-1.31z1@2	Ilmenite	10	25	No	1000	High Ti-Fe, good LREE-I
Lp6ilm-3.10z1@1	Ilmenite	10	20	Slight	1000	High Ti-Fe, good LREE-I
Lp6ilm-3.10z1@2	Ilmenite	10	20	No?	1000	High Ti-Fe, good LREE-I
Lp6mon-1.9z1	Monazite	10	10	Slight	1000	Low Ti-Fe, altered LREE-I
Lp6mon-1.10z1@1	Monazite	8	15	No	1000	Low Ti-Fe, altered LREE-I
2lp6mon-1.10z1@2	Monazite	8	15	Slight	1000	Low Ti-Fe, altered LREE-I
Lp6mon-1.11z1@1	Monazite	15	20	No	2000	Low-Ti-Fe, good LREE-I
lp6mon-1.11z1@2	Monazite	15	20	No	1000	Low Ti-Fe, altered LREE-I
Lp6mon-2.3z1	Monazite	15	25	No	1000	Low Ti-Fe, altered LREE-I
Lp6ap-1.15z1	Apatite	8	8	Yes	1000	Low Ti-Fe, altered LREE-I
Lp6ap-1.27z1	Apatite	6	15	Yes	1000	High Ti-Fe, altered LREE-I
Lp6ap-2.1z1	Apatite	5	15	Yes	1000	Low Ti-Fe, altered LREE-I
Lp6ap-2.36z1	Apatite	10	15	No	1000	Low Ti-Fe, good LREE-I
<i>Butler Peak Granite</i>						
Bbacc-1.18 z1 @1	magnetite	10	40	yes	3000	High Ti-Fe, good LREE-I
Bbacc-1.18 z1 @2	magnetite	10	40	yes	2000	High Ti-Fe, altered LREE-I
Bbacc-1.18 z1 @3	magnetite	10	40	yes	2000	High Ti-Fe, altered LREE-I
Bbacc-1.20 z1 @1	magnetite	10	15	slight	3000	High Ti-Fe, good LREE-I
Bbacc-1.20 z1 @2	magnetite	10	15	slight	2000	High Ti-Fe, good LREE-I
Bbacc-1.21 z1 @1	magnetite	10	10	No	2000	High Fe, good LREE-I
Bbacc-1.2 z1 @1	magnetite	10	20	No	5000	High Ti-Fe, altered LREE-I
Bbacc-1.2 z1 @2	magnetite	10	20	slight	3000	High Ti-Fe, altered LREE-I
Bbacc-1.2 z1 @2, 1 st 2 cycles	Magnetite	10	20	slight	3000	Low Ti-Fe, altered LREE-I

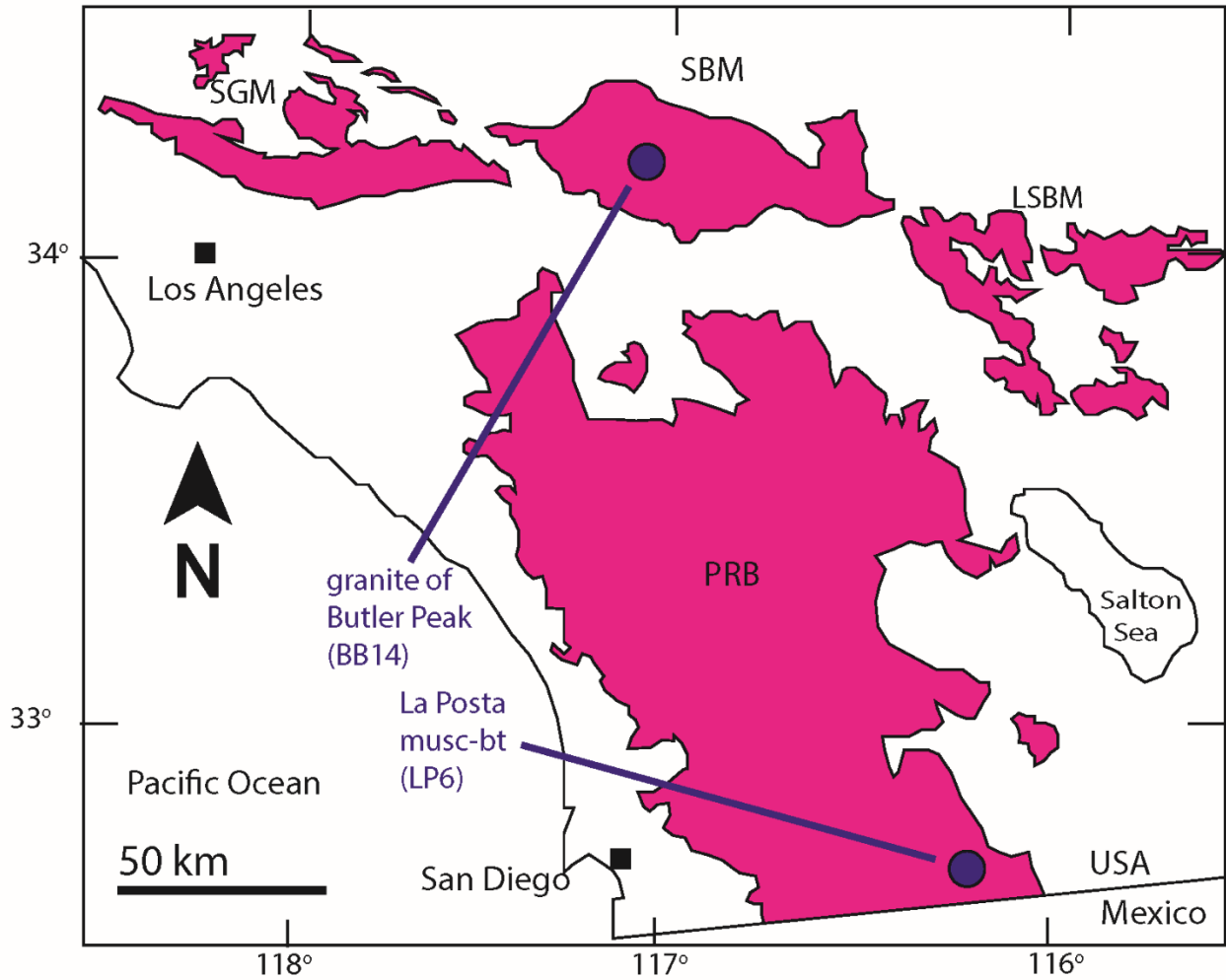
Bbacc-1.2 z2 @1	Magnetite	10	10	No	3000	High Ti-Fe, good LREE-I
Bbacc-3.2 z1 @1	Magnetite	15	20	No	3000	Low Ti-Fe, good LREE-I
Bbacc-3.2 z1 @1	Magnetite	15	20	Slight	5000	High Fe, altered LREE-I
bb14c-ilm-1.13 z1@1	Ilmenite	8	15	Slight	650	High Ti-Fe, good LREE-I
bb14c-ilm-1.13 z1@2	Ilmenite	8	15	Yes	1000	High Ti-Fe, altered LREE-I
Bb14c-ilm-2.14 z1 @1	Ilmenite	8	8	Slight	1000	High Ti-Fe, good LREE-I
Bb14c-ilm-2.24 z1 @1	Ilmenite	10	50	Slight	2000	High Ti-Fe, good LREE-I
Bb14c-ilm-2.24 z1 @2	Ilmenite	10	25	Yes	2000	High Ti-Fe, altered LREE-I
Bb14c-ilm-2.27 z1 @1	Ilmenite	10	30	Slight	2000	High Ti-Fe, good LREE-I
Bb14c-ilm-2.30 z1 @1	Ilmenite	15	25	No	1000	High Ti-Fe, good LREE-I
Bb14c-ilm-2.30 z1 @2	Ilmenite	15	25	No	2000	High Ti-Fe, altered LREE-I
Bb14c-ilm-2.30 z1 @3	Ilmenite	15	25	No	1000	High Ti, good LREE-I
Bb14c-ilm-5.6 z1 @1	Ilmenite	15	25	No	1000	High Ti, good LREE-I
Bb14c-ilm-5.6 z1 @2	Ilmenite	15	25	Slight	700	High Ti-Fe, good LREE-I
Bb14c-ilm-5.6 z2 @1	Ilmenite	10	20	No	1000	High Ti-Fe, altered LREE-I
bb14c-mon-3.5 z1@1	Monazite	5	20	No	1000	High Ti-Fe, altered LREE-I
bb14c-mon-3.22 z1@1	Monazite	6	10	Yes	1000	Low Ti-Fe, altered LREE-I
bb14c-mon-4.7 z1@1	Monazite	15	25	Yes	5000	Low Ti-Fe, altered LREE-I
bb14c-mon-4.7 z1@2	Monazite	15	25	Yes	1000	Low Ti-Fe, altered LREE-I

543

544 Table 1: List of included zircons analyzed for this study along with host phase, size, and degree of spot
545 overlap (if any) with host phase. "Slight" overlap is defined as an off-center part of the shallow, trailing
546 end of the analysis pit overlapping with the host.

547

548

549 **Figure Captions**

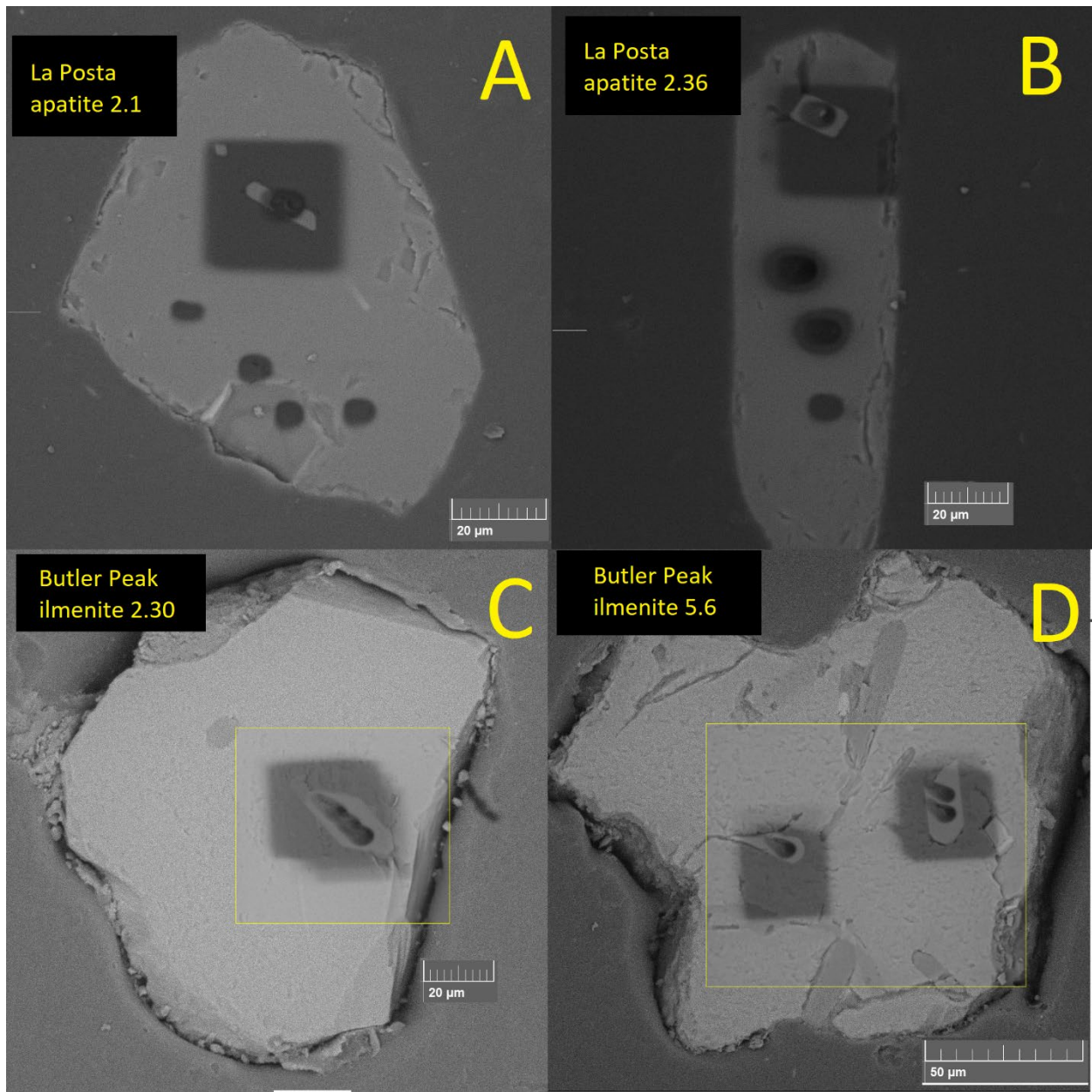
550

551 Figure 1: Map with schematic outlines of southern California batholiths, with sample locations indicated.

552 Associated metamorphic and sedimentary rocks within batholiths not included. SGM: San Gabriel

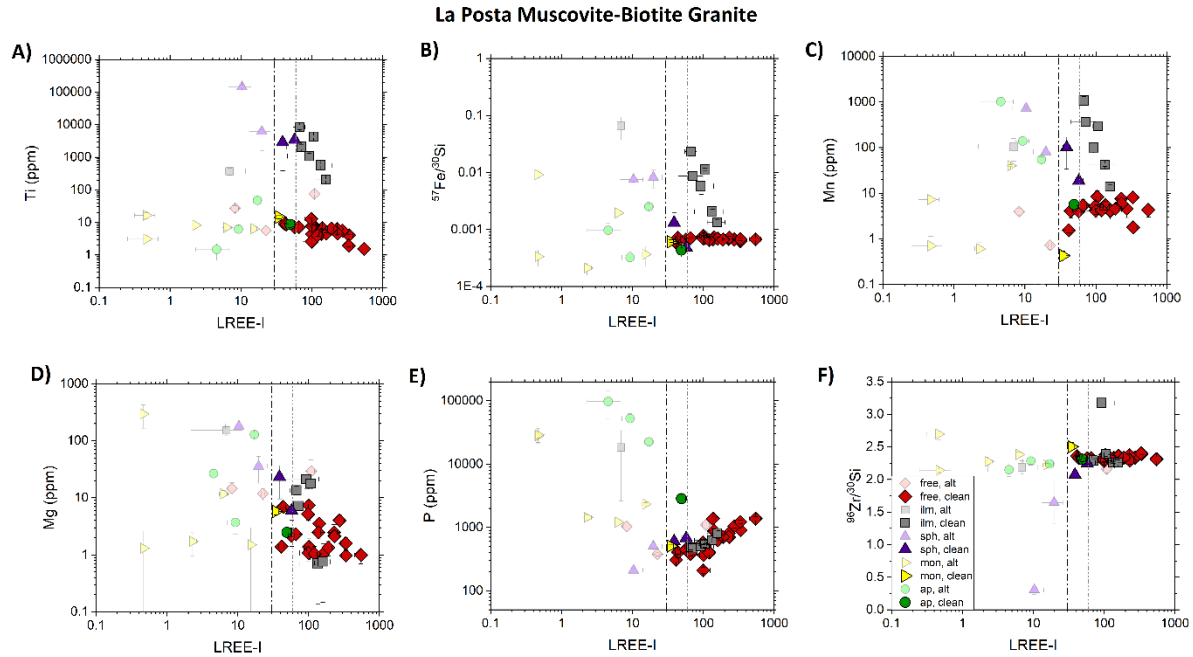
553 Mountains; SBM: San Bernardino Mountains; LSBM: Little San Bernardino Mountains; PRB: Peninsular

554 Ranges Batholith. Modified from Jennings and Gutierrez (2010).



555

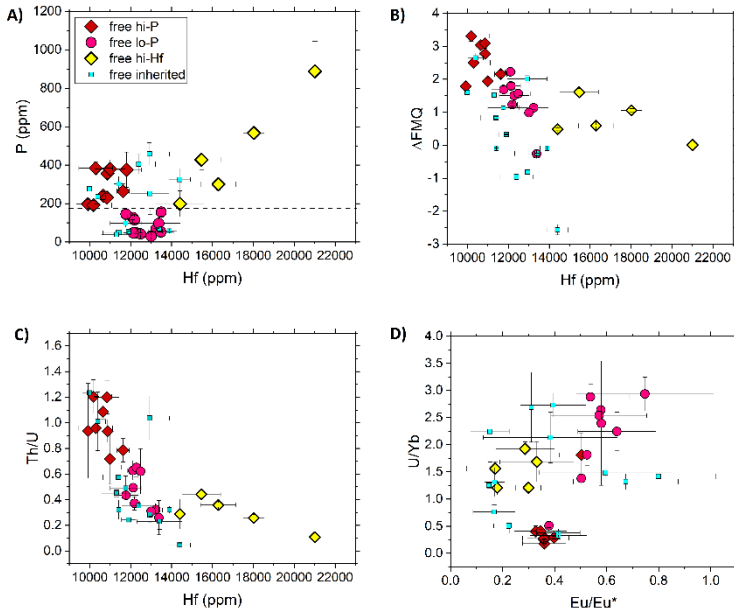
556 Figure 2: Backscattered electron (BSE) images taken after SIMS analysis for several example analytical
 557 spots. Gold coat has not yet been removed from the mount surfaces, allowing the footprint of the
 558 presputtering raster (larger box) to be seen along with the analysis crater. A) & B) zircon in apatite from
 559 the La Posta muscovite-biotite granite; C) & D) zircon in ilmenite from the granite of Butler Peak. Several
 560 test spots and analytical spots on apatite hosts are also shown.



561

562 Figure 3: Measured light element concentrations or ratios to ^{30}Si for La Posta zircons vs LREE-I. Proposed
 563 alteration cutoffs of 30 (Bell et al., 2016) and 60 (Bell et al., 2019) are shown. We consider LREE-I < 30 to
 564 be an “altered” signature for this study. For inclusions, major constituents of the host contaminate all
 565 zircon inclusion analyses even when physical beam overlap is not noted in electron imagery. However,
 566 minor and trace constituents of the host pose little problem. Error bars are 1σ .

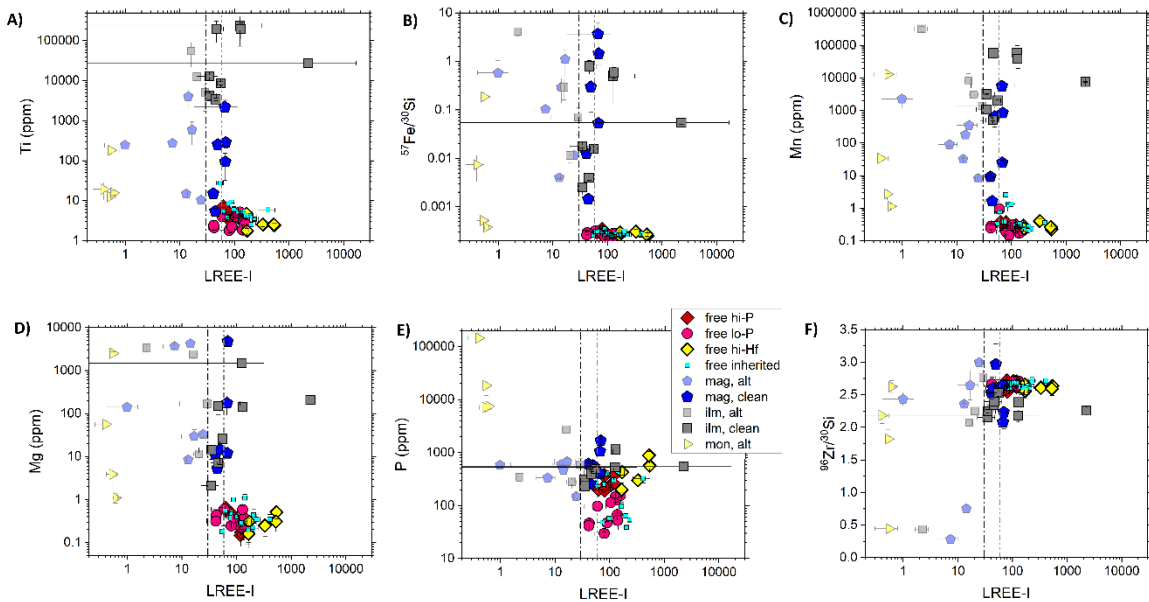
Granite of Butler Peak



567

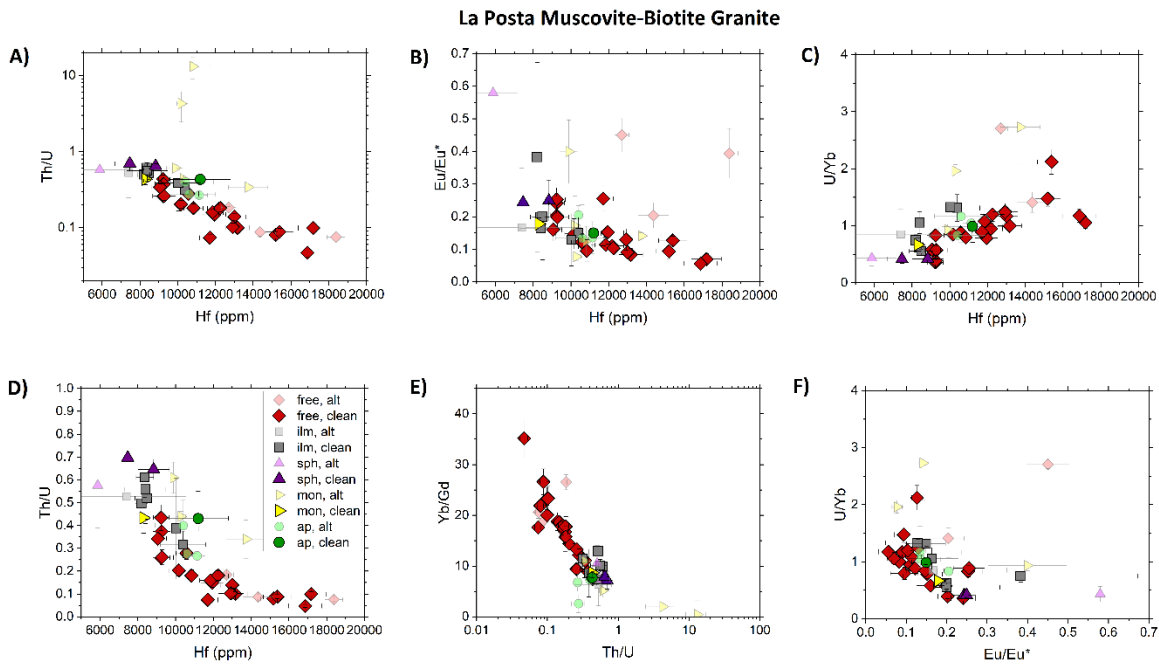
568 Figure 4: Free zircon in the granite of Butler Peak are classified by whether they are inherited or neo-
 569 grown magmatic grains, and the latter are classified into three geochemical groups defined in panel A.
 570 They exhibit a complex chemistry likely involving mixing between less evolved melts represented by the
 571 high-P and low-P groups, which then homogenized to yield the high-Hf group. Error bars are 1σ.

Granite of Butler Peak

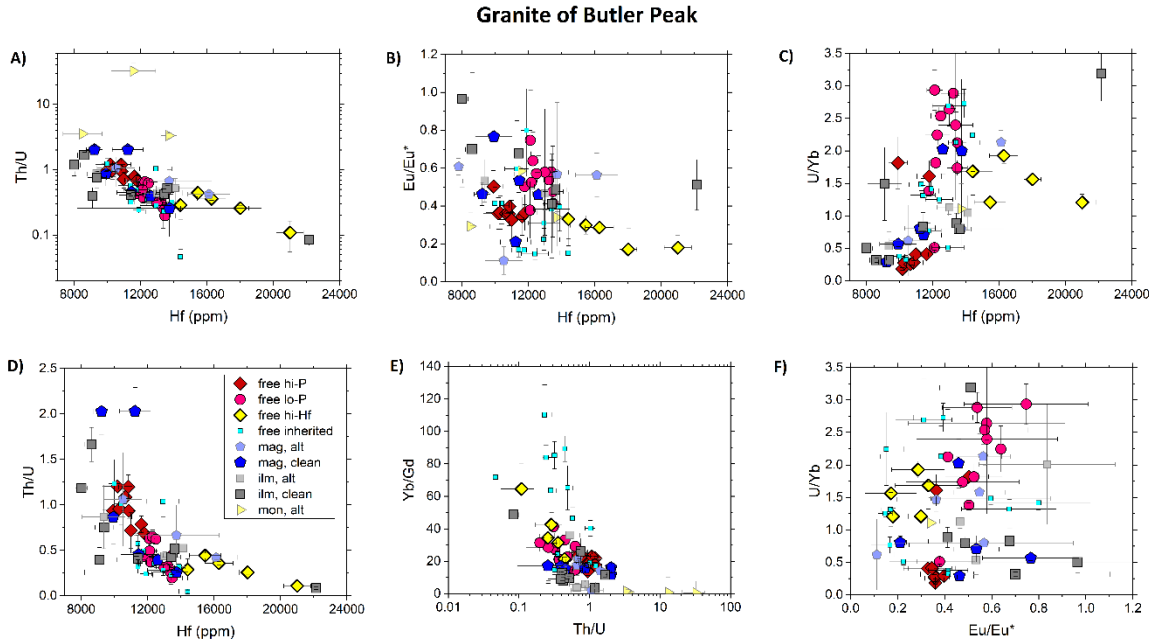


572

573 Figure 5: Measured light element concentrations or ratios to ^{30}Si for Butler Peak zircons vs LREE-I.
 574 Proposed alteration cutoffs of 30 (Bell et al., 2016) and 60 (Bell et al., 2019) are shown. We consider LREE-
 575 I < 30 to be an “altered” signature for this study. For inclusions, major constituents of the host
 576 contaminate all zircon inclusion analyses even when physical beam overlap is not noted in electron
 577 imagery. However, minor constituents of the host pose little problem. Error bars are 1σ .



578
 579 Figure 6: Various magmatic zircon trace element ratios that typically vary during shallow fractionation
 580 plotted for the La Posta muscovite-biotite unit zircons. Legend in panel D applies for all panels. Error bars
 581 are 1σ .



582

583 Figure 7: Various magmatic zircon trace element ratios that typically vary during shallow fractionation

584 plotted for the Butler Peak zircons. Legend in panel D applies for all panels. Error bars are 1σ .